Macromolecules

Article

pubs.acs.org/Macromolecules

Thermomechanical Properties of Bimodal Brush Modified Nanoparticle Composites

Bharath Natarajan,[†] Tony Neely,[‡] Atri Rungta,[‡] Brian C. Benicewicz,[‡] and Linda S. Schadler[†,*]

[†]Department of Materials Science and Engineering, Rensselaer Polytechnic Institute, Troy, New York 12180, United States

[‡]Department of Chemistry and Biochemistry, University of South Carolina, Columbia, South Carolina 29208, United States

Supporting Information

ABSTRACT: The enthalpic incompatibility of organic polymer matrices and high surface energy inorganic nanoparticles often leads to phase separation in polymer nanocomposites (PNC) precluding the realization of anticipated property enhancements. The grafting of polymer chains to nanoparticles holds promise as a means for controlling dispersion. A single population of polymer chains with tunable graft density (σ) and molecular weight (N) is observed to have antithetical enthalpic and entropic effects on interface compatibility. We report the use of bimodal polymer brushes with fundamentally decoupled enthalpic and entropic parameters. Bimodal polystyrene brushes were grafted from 15 nm colloidal silica nanoparticles by a previously reported consecutive RAFT (reversible addition−fragmentation chain transfer) polymerization technique. The combination of a high graft density short brush and a low graft density long brush was found to cause improved nanoparticle dispersion in a polystyrene matrix when compared to single populations of long and short brushes of corresponding graft densities and molecular weights. A new quantitative model was developed to understand these results and was found capable of predicting dispersions in grafted nanoparticle composites in the allophobic dewetting regime. The bimodal-brush-graft particles were also found to be remarkably well dispersed in an entropically unfavorable higher molecular weight matrix. This facilitated a study of the role of matrix−brush entanglement on the thermomechanical properties of PNCs, isolated from the effects of particle dispersion. The best enhancements in glassy properties resulted from improved matrix−brush entanglement, attained by lowering the long chain graft density and increasing the long chain to matrix molecular weight ratio.

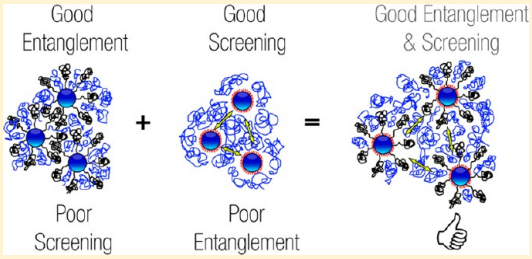

1. INTRODUCTION

The earliest use of covalently tethered curved monomodal polymer brushes was in the stabilization of colloidal suspensions. The entropic repulsion between grafted chains, well wetted by small solvent molecules, was found to prevent flocculation in solution.[1,2] Curved brushes have since been widely explored in polymer nanocomposites (PNCs) as grafted layers on nanoparticle fillers to tailor the nanoparticle/matrix interface.[3,4] Yet, the steric benefits offered by a brush are reduced in PNCs due to the entropic disadvantage of having larger solvent (matrix polymer) molecules.[5,6] These monomodal brush grafted fillers are observed to display distinctly different agglomeration behavior in the high and low graft density regimes when embedded in a homopolymer matrix (Flory−Huggins parameter $\chi = 0$).[7] In the low graft density or allophobic dewetting regime ($\sigma \leq 0.10$ chains/nm^2), the particle core−core van der Waals (vdW) attractions are poorly screened. Given this scenario, with increasing matrix molecular weight, the loss of conformational entropy of the mobile matrix chains begins to gradually outweigh the entropy of mixing with the brush. While the brush and matrix may still be entangled, there is a gentle expulsion of the matrix chains from the brush layer. With a matrix of larger molecular weight than the brush, the poor degree of entanglement does not offer a sufficiently large excluded volume repulsion that would counter the core−core enthalpic attraction. This causes an amphiphile like phase separation into anisotropic structures.[8,9] In the high graft density or autophobic dewetting regime ($(\sigma(N)^{1/2} > (P/N)^{-2}$, where P and N are matrix and brush degrees of polymerization, respectively),[10] although the core−core vdW attractions are presumably well screened, the matrix chains are almost completely expelled from the brush due to a large conformational entropic penalty. This transition from a "wet" to a partially "wet" or "dewet" brush is accompanied by the occurrence of an attractive potential well at intermediate interparticle distances that leads to a mean-field energy at the matrix−brush interface.[5,11−14] Since this isotropic attractive energy is the lowest when brushes contact one another (as in bare particles), these particles form close packed agglomerates to reduce the system free energy.[4,12,15] Sunday et al. presented a comprehensive phase diagram for monomodal polystyrene brush graft silica particles of similar core size (d = 18 nm), exhibiting a relatively small parameter space for achieving good dispersion, bounded by the first order allophobic and second order autophobic dewetting regimes.[16] However, in functional hybrid materials that warrant both a high molecular weight matrix of

Received: March 14, 2013
Revised: May 24, 2013
Published: June 14, 2013

dx.doi.org/10.1021/ma400553c | Macromolecules 2013, 46, 4909−4918

sufficient mechanical integrity and maximal core loading, this parameter space is further limited.

The enthalpic and entropic coupling controls nanoparticle spatial distribution and interfacial entanglement, which in turn strongly dictate the bulk mechanical properties of monomodal-brush-grafted particle filled composites.[17] Allophobic "dewetting" or partial wetting (autophobic) that results in the formation of connected assemblies, leads to the best mechanical reinforcements in the rubbery (high temperature/low frequency) regime.[8,17,18] This solid-like behavior is attributed to the formation of extended particle networks, bridged by interdigitated polymer brushes.[8,12,18,19] The matrix entanglement and the final brush morphology participate negligibly in this enhancement.[17] Under circumstances in which the matrix−brush entanglement is significant, the particles are well dispersed and show little or no reinforcement.[12] However, this entanglement with the matrix brings about the best enhancements in mechanical properties at temperatures below the glass transition temperature (T_g).[19] This is attributed to the presence of a comparatively large volume fraction of positively bound (or entangled) interphase polymer caused by good dispersion and entanglement. Therefore, in monomodal-brush-grafted nanoparticle embedded PNCs, good entanglement (favorable excluded volume repulsion) leads to good dispersion and improvements in the glassy state modulus. Partial wetting or poor entanglement at the interface leads to agglomeration and low modulus due to the low volume fraction of interfacial polymer. This inextricable connection between dispersion morphology and the degree of entanglement has thus far precluded a study of their individual effects on mechanical properties in grafted systems.

In a recent synthesis article, we demonstrated that bimodal particles, i.e., nanoparticles grafted with two monodisperse polymer chain populations of the same chemistry, with decoupled enthalpic and entropic parameters, can alleviate the problem of dispersion optimization.[20] The findings of Li et al.[21] in bimodal-PDMS-grafted TiO_2 homopolymer systems and simulation studies by Jayaraman[22] on polydisperse brushes further support this observation. A versatile, living radical, consecutive-RAFT polymerization technique was employed to synthesize bimodal and/or mixed polymer brush grafted colloidal silica nanoparticles, with control over the chain densities and molecular weights of the two tethered species. In demonstrative experiments, these particles showed superior dispersion and resulted in larger enhancements in glassy-state moduli compared to monomodal particles of similar brush characteristics.[20] Additionally, the bimodal nanoparticles exhibited good dispersion, even at a "dewetting" molecular weight ratio ($P/N = 2$) and tethering density that leads to the formation of agglomerates in conventional monomodal fillers.[8] This suggested that, in these systems, perhaps the effects of the matrix−brush interfacial binding on thermomechanical properties could be studied in isolation from dispersion and vice versa.

In this paper, we elucidate the role of each brush species on dispersion by studying individually, and in combination, long and short brushes of low and high graft densities, respectively. By comparing results from bimodal and monomodal systems with identical entanglement properties (i.e., long brush graft density and effective molecular weight), but with different mesoscale particle structuring, we elucidate the role of dispersion alone on mechanical properties, and by varying the brush graft density and matrix molecular weight in bimodal systems that have near-identical dispersions we isolate the role of the degree of entanglement on the mechanical properties. We also demonstrate an adaptation of the model proposed by Pryamitsyn et al. and Li et al. to accurately predict dispersions for monomodal and bimodal systems ("*monomodal or bimodal*-brush-grafted particle filled PNCs" will henceforth be referred to as "monomodal or bimodal systems" for the sake of brevity).

2. EXPERIMENTAL METHODOLOGY

A. Materials and Synthesis. Monodisperse polystyrene matrices (M_n = 96000 g/mol and 190000 g/mol, PDI 1.01) were procured from TOSOH Biosciences Inc. HPLC grade anhydrous THF was purchased from Fisher Scientific and used without further purification. Colloidal silica nanoparticles (15 nm, 30 wt % in methyl isobutyl ketone (MIBK)) were supplied by Nissan Chemicals Inc. Other materials utilized in the consecutive RAFT polymerization synthesis of grafted nanoparticles have been reported earlier.[20]

The synthesis of bimodal brushes by this consecutive RAFT polymerization process is briefly discussed here. Silica nanoparticles in MIBK were diluted in THF and functionalized with 3-aminopropyldimethylethoxysilane (and trace amounts of octyldimethylmethoxysilane to improve dispersibility). The amine groups in the attached silane molecules were used to anchor activated 4-cyanopentanoic acid dithiobenzoate (CPDB), the chain transfer agent, the tethering density of which was determined using a UV−vis calibration curve constructed from standard solutions of free CPDB. These particles were subsequently surface polymerized with styrene monomer, precipitated into hexanes and redispersed in THF. A small number of particles were set aside and the chains were cleaved using hydrofluoric acid. The molecular weight and polydispersity of the grafted chains were analyzed using a Polymer Laboratories PL-GPC 120 gel-permeation chromatograph (GPC) calibrated with polystyrene standards. Another set of particles were vacuum-dried and analyzed on a TGA to confirm the chain density of the first short brush population (σ_s) based on the molecular weight indicated by the GPC ($M_{n,s}$, kg/mol), using the following equation

$$\sigma_s\left(\frac{\text{chains}}{\text{nm}^2}\right) = \frac{m_p \times N_a}{\left(\frac{100}{\text{TGA weight loss \%}} - 1\right) \times M_{n,s} \times 4\pi r^2} \quad (1)$$

where m_p is the mass of the particle (kg), N_a is the Avogadro number, and r is the radius of the particle. Azobis(isobutyronitrile) (AIBN) with dilauroyl peroxide was used to cleave the RAFT agent off the first population to prevent further reaction during the growth of the second population. The particles grafted with the short brush were refunctionalized with activated CPDB utilizing the unreacted silanols on the silica. The second population was polymerized as described above, dispersed in THF and the molecular weight and polydispersity were determined using GPC. Figure 1 shows the GPC curves for the short brush and bimodal brush grafted PS (σ_s = 0.20 ch/nm^2, $M_{n,s}$ = 6.7 kg/mol, and PDI 1.05 and σ_l = 0.098 ch/nm^2, $M_{n,l}$ = 99.47 kg/mol, and PDI 1.13). A set of particles were again vacuum-dried and analyzed using TGA. The following equation was employed to determine the graft density of the long brush from GPC ($M_{n,l}$) and TGA results.

$$\sigma_l\left(\frac{\text{chains}}{\text{nm}^2}\right) = \frac{m_p \times N_a}{\left(\frac{100}{\text{TGA weight loss \%}} - 1\right) \times M_{n,l} \times 4\pi r^2} - \frac{\sigma_s \times M_{n,s}}{M_{n,l}} \quad (2)$$

Note that the TGA weight loss % indicated here is the percentage of polymer burnt away during the second TGA step, i.e., for the final bimodal brush grafted particles. The monomodal brushes were synthesized and characterized in the same fashion as above, not requiring a second polymerization step.

B. Composite Synthesis. The concentration of particles in THF was determined by boiling off the solvent in a nitrogen purged TGA. The particle solution was rough-mixed with a 5% solution of the desired matrix polymer in anhydrous THF (96000 g/mol or 190000 g/mol) in appropriate quantities. It was then sonicated for 1.5 min at 38%

dx.doi.org/10.1021/ma400553c | *Macromolecules* 2013, 46, 4909−4918

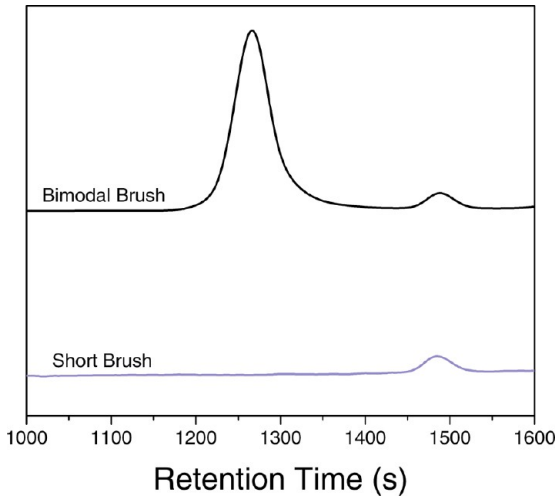

Figure 1. GPC trace of short and bimodal PS chains cleaved from BM10 nanoparticles.

amplitude with a Sonics and Materials Vibracell VCX 600 W unit using a stepped microtip and a 2.0 s ON and 0.5 s OFF pulse. The solution was cast into an aluminum trough and rough dried for 4 h at 80 °C in a clean oven, followed by vacuum drying at 120 °C for 24 h. The dried composite (or neat polymer) was peeled off, broken into pieces and loaded into a dog-bone shaped compression mold. These pieces were pressed into shape at 140 °C with a load of 2 tons and subsequently cooled slowly to room temperature. This sample was then annealed in a vacuum oven at 140 °C, with trace amounts of argon, for 24 h to erase thermal processing history. A small portion of this annealed sample was severed and retained for TGA, DSC, imaging and nanoindentation testing. The remaining gauge section was polished to a parallel thickness ~0.6 mm for DMTA testing. Table 1 shows the characteristics of the

Table 1. Brush Properties of the Various Composites Prepared

	grafted chain			
matrix	molecular weight (kg/mol)	PDI	graft density (chains/nm^2)	composite name
96 kg/mol	7.2	1.04	0.18	BM-05-96
	118	1.19	0.047	
	100	1.14	0.05	ML-05-96
	6.7	1.05	0.20	BM-10-96
	99.47	1.13	0.098	
	99	1.1	0.10	ML-10-96
	7	1.05	0.25	MS-25-96
190 kg/mol	7.2	1.04	0.18	BM-05-190
	118	1.19	0.047	
	6.7	1.05	0.20	BM-10-190
	99.47	1.13	0.098	

various composites studied. Two types of bimodal particles were prepared with roughly the same overall coverage ($\sigma_s + \sigma_l \sim 0.25$ ch/nm^2) and brush molecular weights ($M_{n,s} \sim 7$ kg/mol and $M_{n,l} = 100$ kg/mol), but with varying long brush graft densities of 0.05 chains/nm^2 and 0.10 chains/nm^2 (BM-05 and BM-10, respectively). Two types of monomodal-brush-graft particles with graft densities and molecular weights identical to those of the long brushes of the two bimodal particle types were prepared (ML-05 and ML-10). Additionally a monomodal brush with the molecular weight of the short brush in the bimodal samples (~7 kg/mol) and a graft density equal to the overall coverage (0.25 ch/nm^2) was synthesized (MS-25).

In order to examine the role of the individual brush species on dispersion and to examine the role of dispersion on thermomechanical properties, bimodal and monomodal particles were dispersed in the 96 kg/mol matrix (composites BM-05-96, ML-05-96, BM-10-96, ML-10-96, MS-25-96) at various loadings. To study the role of the degree of entanglement, bimodal particles of the two grafting densities were also dispersed in a matrix of higher molecular weight (190 kg/mol, composites BM-05-190 and BM-10-190) than the effective long brush molecular weight.

C. Microscopy and Image Analysis. The composite was embedded in epoxy and ultramicrotomed into 60−80 nm slices using a diamond knife. A string of these sections were floated onto DI water and collected onto the surface of a copper grid for transmission electron microscopy (TEM). The microstructures were imaged on a JEOL-2010 TEM operating at an accelerating voltage of 200 kV. A qualitative visual assessment of the micrograph is inadequate in identifying subtle differences in dispersion. We therefore quantified dispersion morphologies using the quadrat method.[23,24]

TEM images at 100 000× magnification were found to be representative of the dispersion state (10 000× for MS25-96). These images were binarized and the gray value thresholds were chosen such that the area fraction of the silica cores matched their characterized loadings. The images were then divided into a large number of squares called quadrats, and the number of "particles" in every quadrat (Q) was sampled. Each aggregate was considered as one "particle" with its center of mass at the same coordinates as the center of mass of the aggregate. Skewness is the third moment of the central deviation of the number of "particles" in each cell, and is a measure of the asymmetry in the distribution.[23]

A uniformly dispersed, well distributed system is expected to have a near-zero skewness, as it shows a normal distribution in Q values. A poorly distributed system, on the other hand, is expected to display a large skewness. This is because of a large asymmetry owing to the "particles" being registered only in a small number of quadrats. Additionally, for the same loading, *dispersed* systems are expected to show a higher average Q (Q_{mean}) than aggregated systems, since more "particles" are registered overall in a given number of cells. The choice of cell size is critical in determining these parameters. A cell 3.5−4 times the size of the primary particle is advised and accordingly chosen.[23] The skewness and Q_{mean} values indicated are averages of calculations from two different images.

D. Mechanical Properties. Dynamic mechanical analysis was performed on the polished gauge sections, using a Rheometrics Instruments DMTA-V. One sample per specimen was tested in tension, (The static or the clamping force was 25% in excess of the dynamic force amplitude; this ensured that the samples were never subjected to compression) at a strain of 0.01% to ensure that the loading was elastic. The storage modulus, E', and loss modulus, E'', were recorded as a function of frequency at temperature steps ranging from 70 to 155 °C. Master curves were obtained by time temperature superposition of these isothermal frequency sweeps using the Williams−Landel−Ferry equation.[25] The master curves were further treated using a 10-point adjacent averaging algorithm that removes outliers.

Nanoindentation tests were performed on polished samples using a TI 900 Hysitron TriboIndentor. A 150 nm Berkovich diamond tip, with an area function calibrated on fused quartz, was used for the test. Indents were made in a 3 × 3 square grid at 3 different positions on the sample (27 in all). The indents were load controlled, with each load function consisting of a 10s ramp, 10s dwell and a 10s unloading segment. The peak load within each 3 × 3 grid was varied from 1000 to 2000 μN in steps of 125 μN. The unloading segment was used for reduced modulus calculations. The elastic modulus was obtained from the reduced modulus as described in the literature[26] assuming a modulus and Poisson's ratio of 1141 GPa and 0.07, respectively, for the diamond tip.[27] A Poisson's ratio of 0.34 was used for polystyrene.[28] The errors calculated were standard errors obtained by dividing the standard deviations of moduli with the root number of trials (27).

E. Glass Transition Temperature. The glass transition temperature (T_g) was determined using differential scanning calorimetry (DSC). The samples were subjected to three temperature cycles

dx.doi.org/10.1021/ma400553c | Macromolecules 2013, 46, 4909−4918

between 25 and 130 °C, with heating and cooling rates of 10 °C/min. The inflection point of the heat flow curve during heating was considered the T_g. The average T_g from the second and third cycles was taken to be the T_g of the sample. The average from 2 samples was taken to be the final T_g.

3. RESULTS AND DISCUSSION

A. Dispersion Behavior. Figure 2 shows a representative set of dispersions demonstrating the advantage of grafting bimodal brushes. The micrographs of the short high density brush grafted monomodal particles (MS-25) dispersed in the 96 kg/mol matrix show that these particles organize into micrometer-sized agglomerates that grow in volume with increased particle loading. This agglomeration is attributed to the entropic (conformational) penalty of the matrix mixing with a dense brush of much smaller molecular weight ($P/N \sim 13.5$). The positive surface tension that arises out of this imbalance leads to a net attraction between brushes, even when the core enthalpies are well screened.[10,29] This observation corroborates well with the dispersions reported for similar values of σ and P/N by Chevigny et al.[15] and in addition, fits into the autophobic dewetting regime of the empirical phase diagram developed by Sunday et al.[16] (dewetting phase begins at $P/N \geq 4.3$ for $\sigma = 0.28$ ch/nm^2). Note that in order to frame the large clusters within the micrographs, magnifications had to be low (20 000×) for MS-25-96. Figure 2 also shows the dispersions of the 5 silica wt % long brush grafted monomodal particles at σ = 0.05 and 0.1 ch/nm^2 (ML-05 and ML-10) in the 96 kg/mol matrix at 100 000×. The dispersion of long monomodal brush graft particles was far superior to the dispersion of the short brush graft particles. They also display self-assembly into anisotropic agglomerates that grow laterally with the addition of particles (dispersion images at higher loadings can be found in the Supporting Information) for both graft densities. These microstructures are as suggested by the 'morphology' diagram developed by Akcora et al.[8] and are well placed in the allophobic dewetting regime of Sunday et al.'s phase diagram.[16]

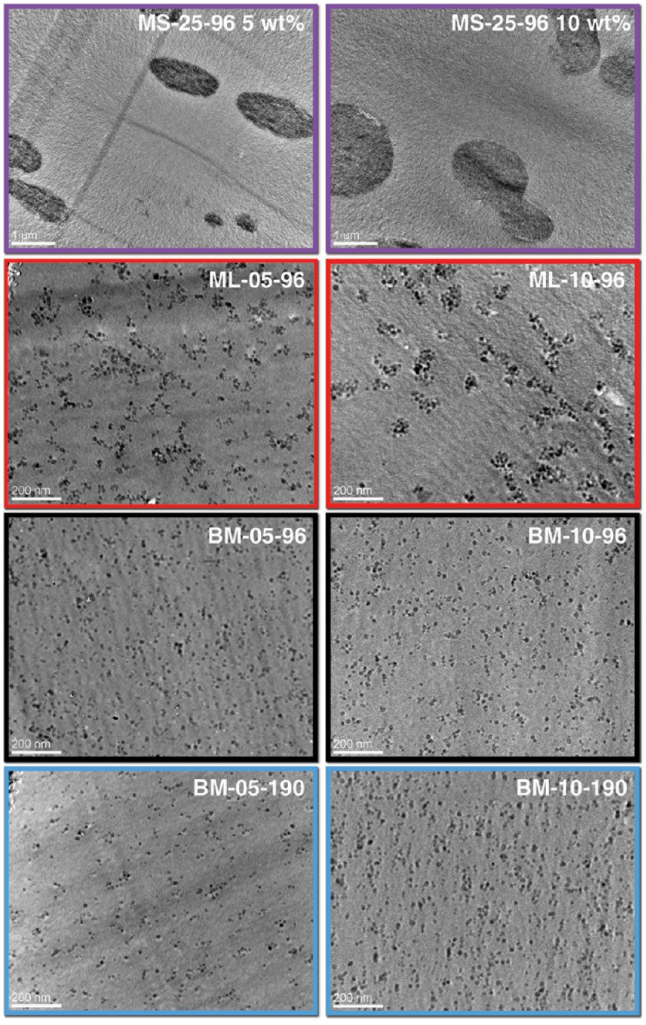

Figure 2. TEM micrographs of silica loadings of 5 wt % (except when indicated otherwise) of the various systems at 100 000× magnification (20 000× for MS-25-96 systems).

From Figure 2, we see that the combination of the long and short brush causes a significant improvement in dispersion, for both σ_l = 0.05 and 0.1 ch/nm^2, in the 96 kg/mol matrix (BM-05-96, BM-10-96). Remarkably the particles remain well dispersed even in a matrix of much larger molecular weight 190 kg/mol (BM-05-190, BM-10-190), for which there is a stronger entropic drive to agglomerate.[8]

These dispersions are quantified as described earlier to obtain the skewness and Q_{mean} and plotted versus the concentration of silica (wt %) (Figure 3). These plots confirm the qualitative inferences made from the micrographs in Figure 2. At all loadings, the bimodal systems exhibit lower skewness values (Figure 3a) than the monomodal systems suggesting that they have a superior distribution of particles. Additionally, the Q_{mean} for the bimodal systems at every loading is much higher than that of the monomodal systems indicating that there are more individually dispersed particles (Figure 3b). These plots reveal that all the bimodal systems are better distributed and more uniformly dispersed than the monomodal particles. The skewness is found to increase with decreasing loading. This is because, for the same cell size and quality of dispersion, at lower loadings fewer quadrats register particles. Q_{mean}, on the other hand, increases with loading because more particles are registered for the same number of cells. Since the dispersions in MS-25-96 are manifestly poor, their skewness (>10) and Q_{mean} ($\sim 10^{-4}$) are not plotted.

We attribute the improvement in dispersion in the bimodal composites to the addition of a dense short brush to the long brush population (or conversely, the addition of a few long chains to the dense short brush population). Both of these points of view have significant qualitative support in literature. The former is as per the findings of Pryamitsyn et al.,[9] which suggest that a lowered enthalpic gain of core aggregation leads to an improved probability of dispersion. The latter is in accordance with simulation results, which suggest that addition of a small number of "wettable" long chains to a dense brush (i.e., the bimodal limit of polydispersity) abates the attractive energy well between particles at transitional distances.[22,30,31] Evidently the combination of the two brushes tenders enough enthalpic screening and entropic excluded volume repulsion to keep these particles well dispersed in both the 96 kg/mol and 190 kg/mol matrices.

In order to further explain these results quantitatively, a predictive phase diagram incorporating enthalpic and entropic contributions to dispersion was sought. Li et al. have developed a predictive tool of this nature based on the parametric phase diagram simulated by Pryamitsyn et al.[9,21] The modus operandi of developing such a phase diagram involves calculating the free energy (F_{flat}) and height of a chain (h) in a flat brush, of identical

dx.doi.org/10.1021/ma400553c | Macromolecules 2013, 46, 4909−4918

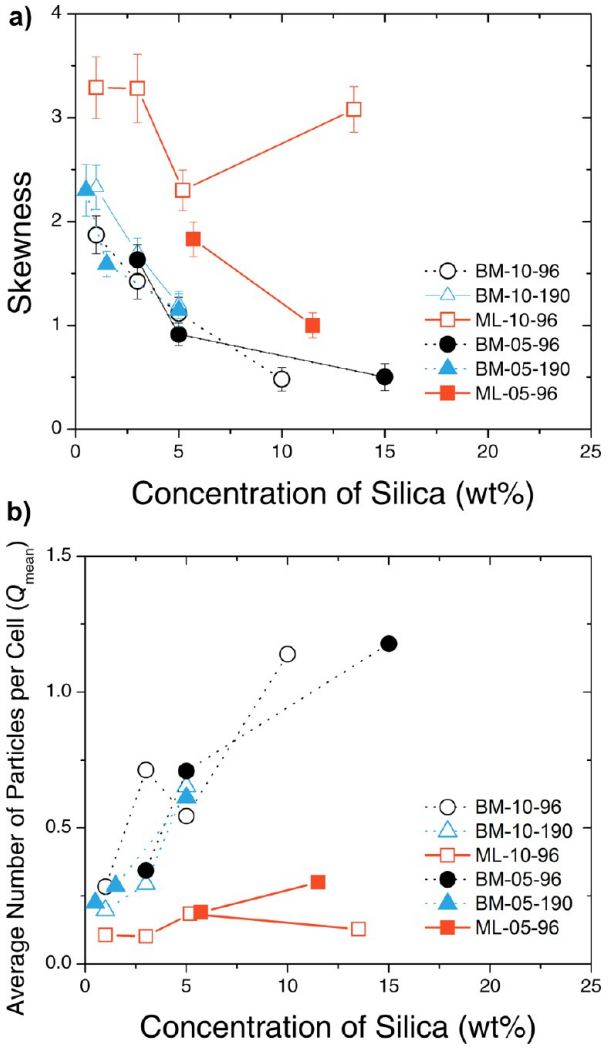

Figure 3. (a) Skewness vs silica weight % and (b) average number of particles per cell (Q_{mean}) vs silica weight %, for systems under our purview. Note that the lines serve merely to guide the eye.

characteristics as the grafted brush of interest (N, σ). These values are then transformed to obtain the free energy of the chain in cylindrical (strings, C), spherical (dispersed, D) and sheet like (H) morphologies. In aggregated systems (A), the free energy of a chain is calculated based on the assumption that it is compressed into a gap on the order of the radius of the particle. The boundaries separating the various phases are identified by balancing the conformational energy of the chain and the enthalpic gain of agglomeration per chain.

In the work of Li et al., the enthalpic component was calculated from the van der Waals interaction energy between two (effective) particle cores interacting in a polymeric medium.[21] Using a similar methodology, for monomodal brush grafted particles, we estimated the vdW energy (χ) between cores with the attached surface modifier (unreacted octyldimethylmethoxysilane) from the Hamaker constants of the pristine particle, the octylsilane and the matrix polystyrene using the formalism developed by Vold.[32] For bimodal particles, the vdW energy was obtained as before, while considering the short brush and the octylsilane, together as a hybrid modifying layer of effective refractive index and dielectric constant.[33] These calculations can be found in section B of the Supporting Information. The addition of the short brush population was observed to significantly decrease the intercore attraction from $5k_BT$ to $0.19k_BT$.

For the entropic contributions, the scaling relations used by Pryamitsyn et al. and Li et al. were found to overestimate the values of the flat brush height ($h = Na^{2/3}\sigma^{1/3}\upsilon^{1/3}$) and free energy $F = Na^{2/3}\sigma^{5/6}\upsilon^{1/3}$ for this range of N and σ (a is the monomer size =0.56 nm for PS[34] and υ is the excluded volume parameter).[9,21] Their assumption that $\upsilon = a^3N/P$, leads h and F to scale as $\sim N^{4/3}$, whereas the scaling law established in the literature is $\sim N$ for flat brushes.[35] It is suggested by Li et al. that applicability of their model is limited to low grafting densities and molecular weights.[21] We developed a modified model to extend the predictive ability to larger molecular weights and intermediate grafting densities. In order to do so, different expressions for brush height and energy were adopted.

An expression for the height, h, of a stretched flat polymer brush in a chemically identical melt was developed by Aubouy et al. $h = Na^{5/3}\sigma^{1/3}p^{-1/3}$.[36,37] The values predicted by this scaling relation were found to be realistic when compared to the experimentally measured values of grafted brush heights in homopolymer melts.[15] The calculated value of h was further used to estimate the repulsive energy between two flat brushes (ϕ) based on the equation derived by Milner[38] and Mewis et al.[39]

$$\frac{\phi}{k_BT} = \frac{\pi^2}{24}\frac{h^2\sigma}{Na^2}\left[\frac{2h}{d} + 2\left(\frac{d}{2h}\right)^2 - \frac{1}{5}\left(\frac{d}{2h}\right)^5 - \frac{9}{5}\right] \quad (3)$$

where k_B is the Boltzmann constant, T is the temperature and d is the distance between the grafted surfaces. This energy was further divided by the number of chains per particle (n_p) to obtain the interaction energy per chain of a flat brush ($F_{flat} = \phi/k_BTn_p$).

The flat brush energy per chain (F_{flat}) and height (h) were used in the expressions derived by Zhulina et al,[40] as in the Pryamitsyn model,[9] to estimate the energies of a chain grafted on spherical (dispersed), cylindrical (strings) and sheet like substrate morphologies. A modified excluded volume parameter was employed in the equation suggested by Pryamitsyn et al.[9] to obtain the free energy of a compressed chain in an aggregate. The boundaries between dispersed, string-like, sheet-like and aggregated systems were identified by balancing the system energies (conformational energy per chain + enthalpic gain of contact per chain) of neighboring phases. The details of these calculations can be found in the Supporting Information. In a homopolymer system, for a fixed matrix molecular weight, particle size and enthalpic attraction, the only variables are N and σ. The information from these equations (Supporting Information) can therefore be recast as plots of dimensionless parameters n_p and R/R_g, which are simple functions of N and σ.

The phase diagrams generated for the monomodal and bimodal systems are shown in Figure 4, parts a and b. The trends in the diagrams are quite clear. For a constant particle size, R, and constant chain length, N ($\sim R_g$), the tendency to disperse increases with an increase in the number of chains (n_p). For a constant particle size, R, and constant n_p, the dispersion improves with an increase in the chain length ($\sim R_g$). Additionally the agglomeration regime grows with increasing P. The phase boundary is found to shift favorably toward a higher probability of a dispersed phase for the bimodal systems. It is observed that the diagram is able to predict the dispersion morphology of both monomodal and bimodal particles. The monomodal brush graft particles embedded in a 96 kg/mol matrix lie in the strings (C) region of the phase diagram, whereas bimodal brush graft

dx.doi.org/10.1021/ma400553c | Macromolecules 2013, 46, 4909−4918

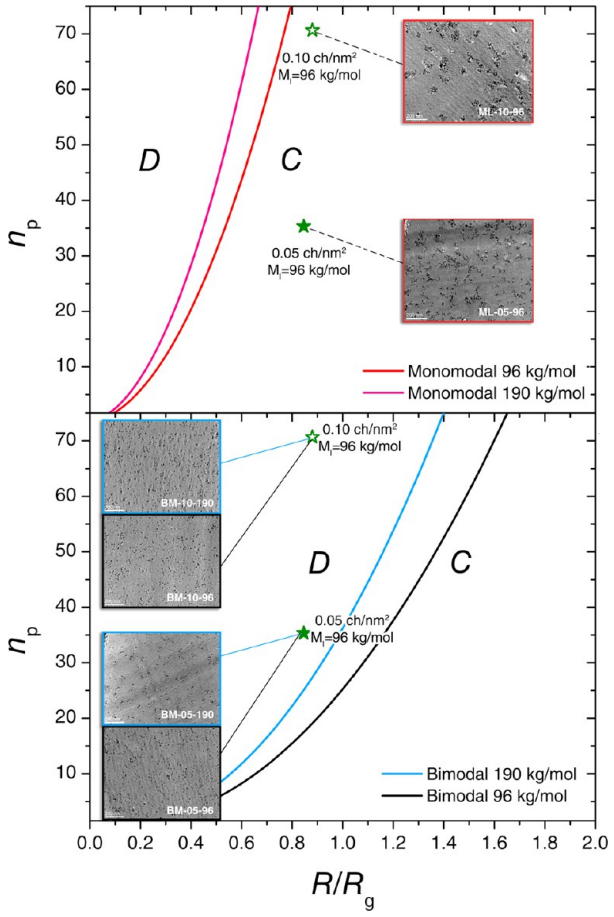

Figure 4. Parametric phase diagram of the homopolymer PS−silica: (a) monomodal and (b) bimodal systems under our purview, showing the dispersed and string-like agglomerate regions. The experimental micrographs of 5 wt % silica loadings of the samples are shown to demonstrate the validity of the predictions. The open and filled stars correspond to grafting densities of 0.10 ch/nm^2 ($n_p \sim 71$) and 0.05 ch/nm^2 ($n_p \sim 35$). The monomodal 190 kg/mol boundary is shown purely to illustrate the shift in phase boundaries with varying matrix molecular weight. The dotted lines serve to merely guide the eye.

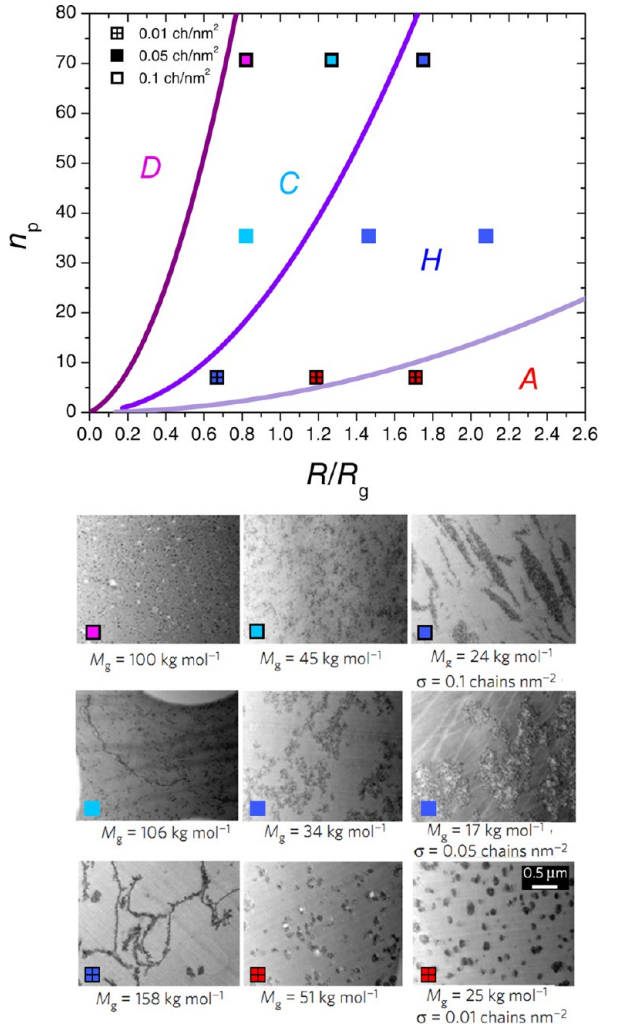

Figure 5. Parametric phase diagram for a matrix of molecular weight 142000 g/mol from Ackora et al.[8] The various points on the plot correspond to various grafted chain molecular weights ($\sim R_g$) and grafting densities (σ).

particles lie in the dispersed region (D) corresponding to their phase boundary. This observation is also true of the 0.1 ch/nm^2 particles and 190 kg/mol matrix bimodal systems.

Apart from using the diagram to quantitatively predict the dispersions in our study, we applied it to predict the dispersions from Akcora et al.[8] (Figures 5 and 6). The predictions made are found to be in excellent agreement with their experimental results, even while neglecting effects of polydispersity and other subtleties of sample preparation. It is noted that, while certain predicted morphologies might be misplaced from the phase suggested by their micrographs, these deviations are only minor. Additionally since the transition of morphologies from dispersed → strings → sheets → aggregated is smooth, it is difficult to identify the structuring of certain particles as belonging to only one of the aforementioned phases. Intermediate morphologies like dispersed strings or strings of sheet-like aggregates may be observed near the phase boundaries.

B. Mechanical Behavior. *Role of Dispersion.* The mechanical properties of all the composite types were investigated at various concentrations of silica. The viscoelastic properties, measured through isothermal frequency sweeps on the DMTA, are shown in representative plots in Figure 7. Figure 7a shows the glassy state storage moduli of 5 wt % silica loadings ML-10, BM-10, ML-05 and BM-05 in the 96 kg/mol matrix. The neat polymer curve is also plotted for reference. These curves were obtained by frequency shifting of master curves such that the peak loss moduli corresponding to glass transition coincided. This T_g normalization was performed in order to make a true comparison of glassy properties at identical decades of frequency away from the glass transition temperature. The 4−6 decade regime (0 being T_g) shown in Figure 7a corresponds to temperatures 10−15 °C less than T_g. It is evident from Figure 7a, when comparing glassy state mechanical properties of BM-10-96 and ML-10-96 and of BM-05-96 and ML-05-96, that the enhancement following the addition of bimodal particles is greater than that presented by the monomodal particles for each of the graft densities.

This enhancement is further investigated by static nanoindentation tests at room temperature. The elastic modulus is calculated from the reduced modulus, as described earlier.[26] The results of the indentation experiments are represented in Figure 8, as plots of the normalized modulus versus silica weight loadings. The trends observed in the DMTA data in Figure 7 are in agreement with those in Figure 8. This is found to be true at all intermediate loadings. Additionally, the bimodal results are

dx.doi.org/10.1021/ma400553c | Macromolecules 2013, 46, 4909−4918

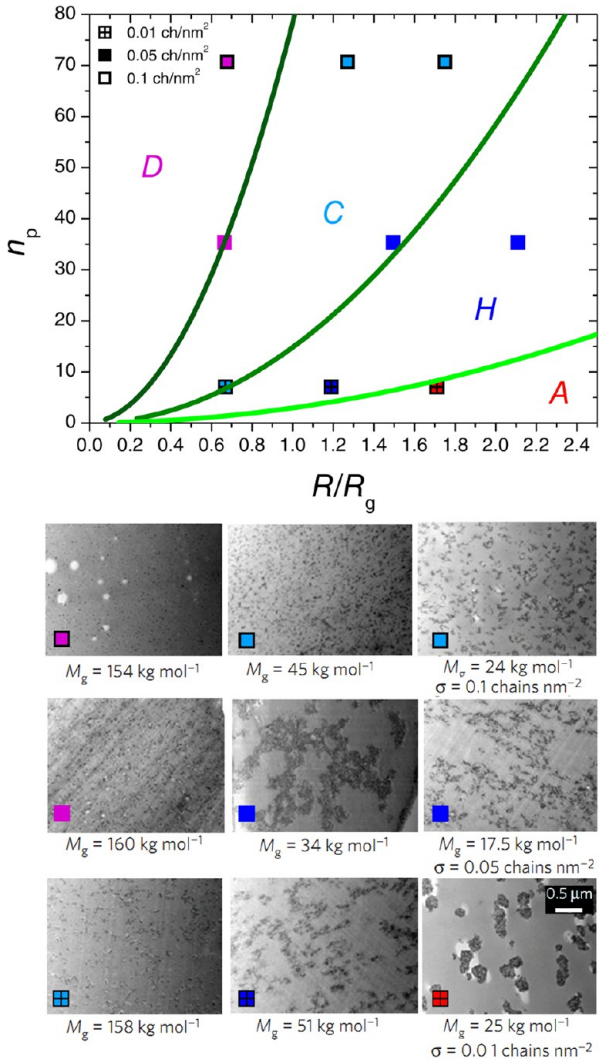

Figure 6. Parametric phase diagram for a matrix of molecular weight 42000 g/mol from Ackora et al.[8] The various points on the plot correspond to various grafted chain molecular weights ($\sim R_g$) and grafting densities (σ).

found to be far superior to the predictions made by the Halpin–Tsai[41] ($E_{silica} \sim 70$ GPa) and Guth[42] micromechanical models. The Guth equation predicts larger enhancements in modulus as it considers interactions between particles at higher loadings.[43] The results for the monodisperse particles closely follow the Guth predicted trend.

We attribute this larger enhancement offered by the bimodal particles to their superior dispersion state, while still maintaining the same entanglement effects ($Skewness_{BM\text{-}10\text{-}96} < Skewness_{ML\text{-}10\text{-}96}$, $Skewness_{BM\text{-}05\text{-}96} < Skewness_{ML\text{-}05\text{-}96}$). These observations are in accordance with those reported by Maillard et al.,[19] who noted that dispersion plays contrasting roles in optimizing low and high temperature mechanical properties. The largest increase in glassy properties such as the elastic modulus was observed in the best dispersed system. This follows from the notion that better dispersed systems benefit from a larger interfacial surface to volume ratio.[44] We have thus, for the first time, been able to observe the role of dispersion in grafted systems while maintaining the same entanglement properties ($E_{BM\text{-}10\text{-}96} > E_{ML\text{-}10\text{-}96}$, $E_{BM\text{-}05\text{-}96} > E_{ML\text{-}05\text{-}96}$).

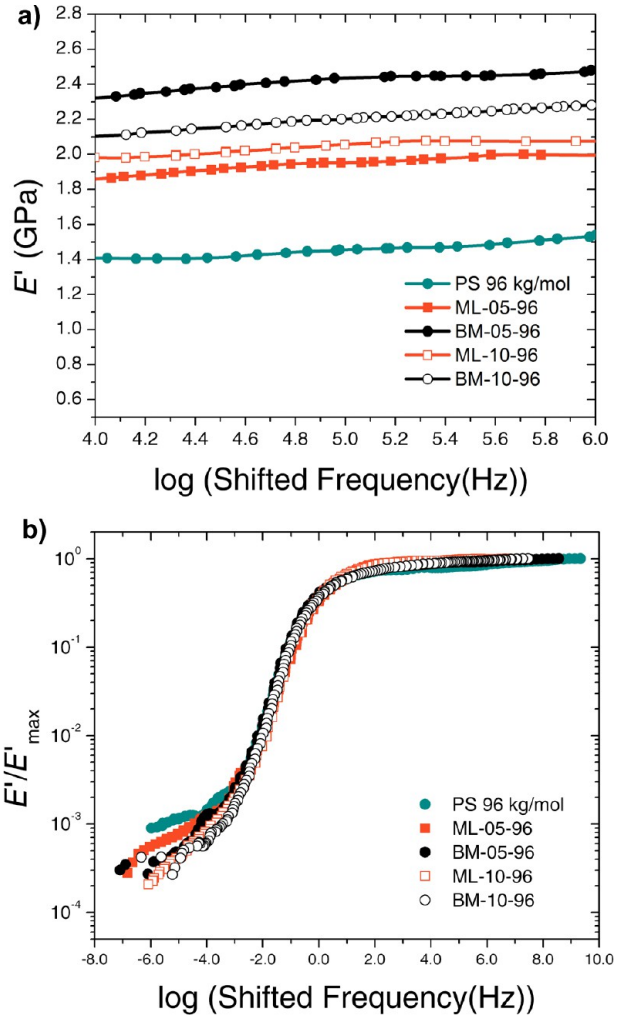

Figure 7. (a) Storage modulus E' (GPa) vs log (shifted frequency (Hz)) for 5 wt % silica loadings of various systems compared with neat 96 kg/mol PS. (b) Normalized storage modulus E'/E'_{max} vs log (shifted frequency (in Hz)) for 5 wt % silica loadings of various systems compared with neat 96 kg/mol PS.

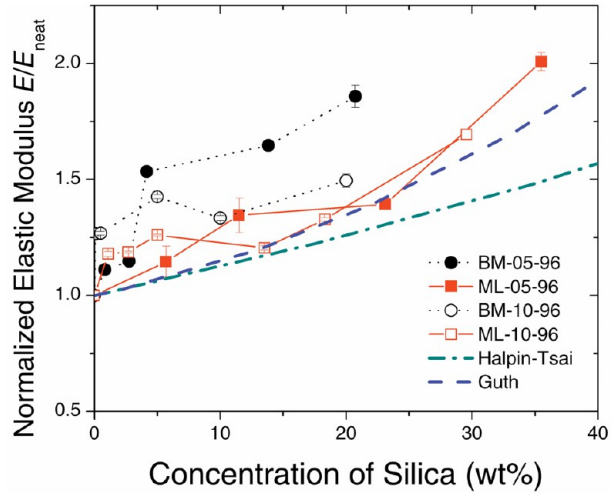

Figure 8. Elastic modulus normalized by pure polymer modulus E/E_{neat} vs silica concentration (wt %) for various systems compared with the Halpin–Tsai and Guth predictions for silica in the 96 kg/mol matrix.

dx.doi.org/10.1021/ma400553c | Macromolecules 2013, 46, 4909–4918

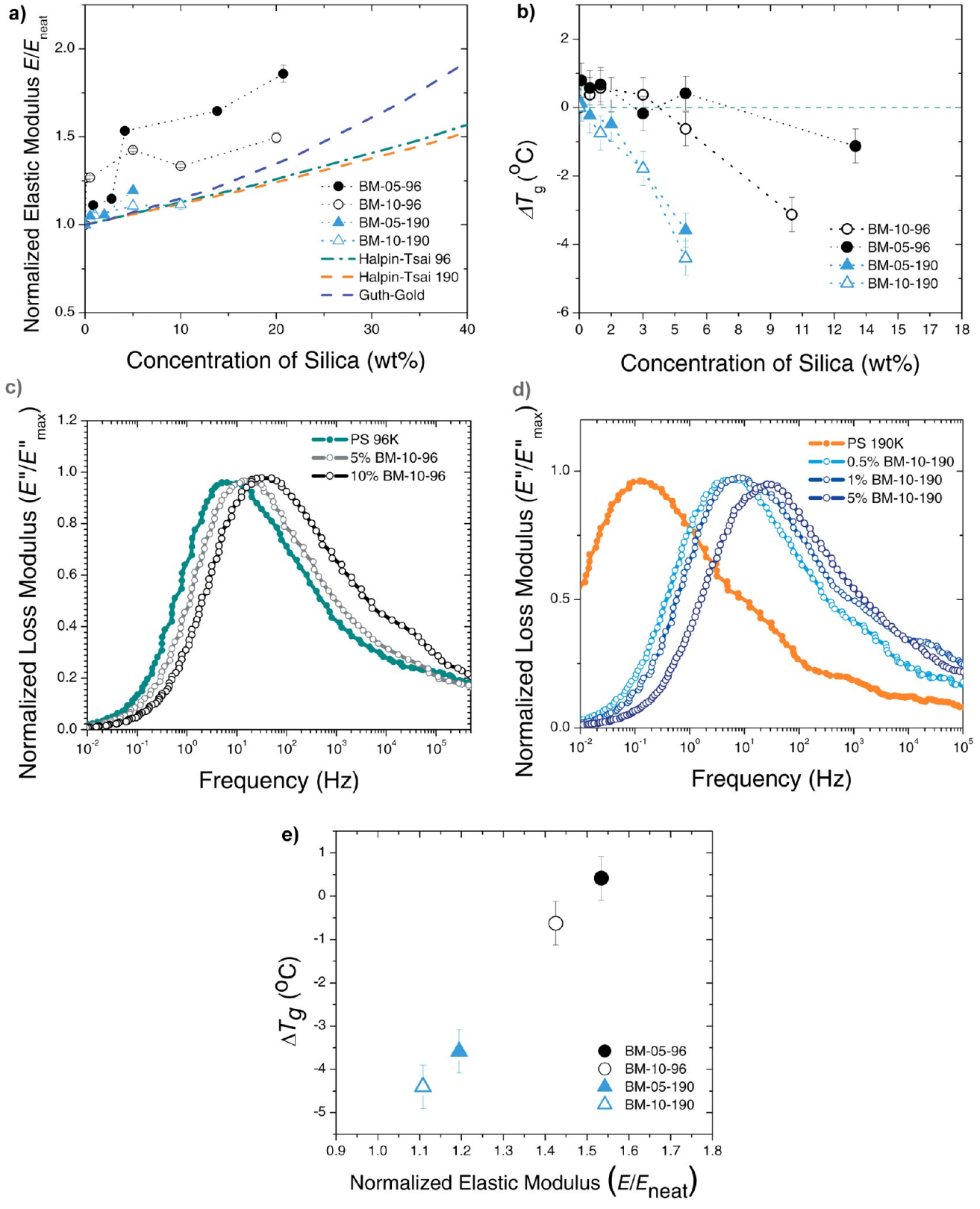

Figure 9. (a) Elastic modulus normalized by pure polymer modulus E/E_{neat} vs silica concentration (wt %) for bimodal systems, compared with the Halpin−Tsai and Guth predictions. (b) ΔT_g (°C) vs silica weight % for bimodal systems. (c and d) Normalized loss modulus curves in BM-10-96 and BM-10-190, respectively, showing a shift in loss modulus peak to higher frequencies with increased loading. A positive frequency shift in glass transition is equivalent to a negative shift in T_g. (e) Plot of normalized elastic modulus vs ΔT_g at 5 wt % silica loadings of the various systems.

Additionally we observe that the there is no significant impact on high temperature mechanical reinforcement in the bimodal and monomodal systems. A representative plot of this observation is shown in Figure 7b. Here the frequency shifted moduli, scaled down by the neat polymer modulus, are all found to overlap; that is to say they that all possess the same shape as a

dx.doi.org/10.1021/ma400553c | *Macromolecules* 2013, 46, 4909−4918

function of frequency. The lack of reinforcement is also seen within all the systems at nearly all loadings of silica. The bimodal systems are well dispersed, with no stress propagating interparticle bridges.[17,18] In the monomodal systems, the anisotropic aggregates are found not to be extending through the sample and neither are there any glassy bridges (PS and silica have a repulsive interface).[18,45] The only system showing reinforcement is ML-05-96 (35.5% silica by weight). We attribute this observation to the physical constraints imposed on the matrix chains at such a high loading (see section C of the Supporting Information).

Role of Brush−Matrix Entanglement. As has been shown earlier, the dispersions in all the bimodal systems are qualitatively and quantitatively similar. Therefore, any divergence in the normalized mechanical properties is to be attributed to the differences in the degree of brush matrix entanglement. Nanoindentation tests (Figure 9a) reveal that the bimodal particles offer a larger elastic modulus augmentation in the 96 kg/mol matrix when compared to the enhancements in the larger molecular weight 190 kg/mol matrix, which show only a marginal improvement, if any, over the Halpin−Tsai predictions. We also observe that as the graft density increases, the increase in modulus decreases. These observations suggest that the poorer the entanglement of the matrix chains, the lower the modulus. We test the same by measuring the T_g in these systems, since T_g has been established as being indicative of entanglement behavior in grafted systems.[46,47] The T_g shifts are shown in Figure 9b. We note that shifts in DMTA peaks are well correlated with the T_g as shown by a representative plots for BM-10-96 and BM-10-190 (Figure 9c and 9d).

The T_g drops (∼3 °C at 10 wt % silica) following the addition of σ_l = 0.1 ch/nm^2 bimodal particles to the 96 kg/mol (BM-10-96), are found to be higher than those in the 0.05 ch/nm^2 system, which shows no change in T_g. The T_g drops induced in the 190 kg/mol matrix are much higher than the drops in the 96 kg/mol matrix. While this lowering of T_g in the 190 kg/mol could be due to the plasticizing effect of a lower molecular weight 100 kg/mol chains,[48] we rule this out since the 100 kg/mol and 190 kg/mol have similar T_gs.

It has been established that the glass transition temperature in athermal graft polymer−matrix systems can be increased or decreased when the matrix chains entangle favorably or poorly with the brush, respectively.[6,49] When the matrix chains are partially entangled,[10] they experience a lowered friction leading to faster relaxation times expressed in bulk as lowered T_gs.[49,50] Ferreira et al. have identified a boundary for such "dewetting" for sparse brushes using self-consistent field analysis.[10] This boundary is defined by $\sigma\sqrt{N} > (P/N)^{-2.0}$ i.e., entanglement is poorer for a larger value of the ratio $\sigma P^2/N^{3/2}$. This ratio is calculated for the systems under our purview: BM-05-96 (1.23), BM-10-96 (3.13), BM-05-190 (5.27), and BM-10-190 (12.29). Since this boundary is defined for flat brushes, the condition is expected to be relaxed for spherical brushes in which the volume available increases with increased distance from the particles.[51] Nevertheless, the value of the ratio is comparable to unity only for the BM-05-96 system, and increases with increasing graft density and matrix molecular weight. We are therefore led to conclude that the 96 kg/mol matrix is reasonably well entangled with the 0.05 ch/nm^2 brush, and less entangled with the 0.10 ch/nm^2 brush. As the matrix molecular weight is increased above the brush molecular weight, the entanglement worsens. With poorer entanglement, the matrix chains enjoy a lower interfacial friction, thereby leading to the observed drops in T_g. Furthermore, since the particles that cause "dewetting" act as plasticizers in the matrix, they are found to not induce the same amount of modulus enhancement as particles that show strong interfacial binding. To further support the view that for the same dispersion state, glassy state property enhancements in grafted particle filled PNCs are strongly dictated by the extent of entanglement, we plot the ΔT_g vs normalized elastic modulus for 5 wt % silica loading (Figure 9e). This graph reveals a remarkable correlation that confirms this notion. We have therefore been able to characterize the influence of brush−matrix entanglement on the mechanical properties of grafted particle filled systems, for the first time isolating the effects of dispersion.

4. CONCLUDING REMARKS

While the grafting of monodisperse polymer chains to particles holds potential in tuning particle polymer interfaces, the enthalpic and entropic coupling in these systems limits the ability to tailor both dispersion and mechanical properties independently. We have convincingly shown through experiments that combining a long entangling brush and a short screening brush leads to excellent dispersion and holds a definite advantage over the individual brush species in homopolymer systems. In order verify these results, we developed a new model that extends the predictability of earlier phase diagram approaches to intermediate grafting densities and large molecular weights. It is seen from these phase diagrams that the addition of the screening short brush greatly expands the parameter space of good dispersion by lowering core−core enthalpy. Our quantitative model is found to predict the dispersions in our systems and those from the work of Akcora et al. to a good degree of accuracy. The model can be extended to study other filler-grafted polymer systems and represents a significant step toward being able to predict and design dispersions in grafted particle composites.

The energetic pairing in monomodal systems causes the dispersion and matrix−brush entanglement to be linked, i.e., the extent to which the matrix penetrates the brush determines the dispersion state. Through the use of bimodal brushes, we have been able to study the effects of these important factors separately. By tuning the enthalpic screening, for constant long chain grafting densities, we have been able to manipulate dispersion and show the effect of dispersion on mechanical properties isolated from entanglement effects. Better dispersed systems show greater enhancements in glassy properties for the same quality of interface. This is attributed to the presence of a larger volume fraction of interfacial polymer that results from superior dispersion.

By tuning the entanglement, for near identical dispersion states, we have shown that the best modulus enhancements occur with the highest interfacial binding. Systems where matrix chains experience low friction at the brush-matrix interface, did not exhibit any significant enhancements in glassy state properties. We have for the first time been able to study interfacial effects in grafted systems without having to account for dispersion during comparison. This is analogous to the investigation of thin films coated on grafted substrates, where the thin film dimensions (equivalent to inter particle distances) can be predetermined. This bimodal ideology and the phase diagram approach can be used in conjunction to accurately study the hybrid particle−matrix interface and the independent role of interfacial polymer properties on bulk properties in grafted particle filled functional PNCs.

■ ASSOCIATED CONTENT

Supporting Information

Dispersion at higher loading, theoretical considerations, and reinforcement at high loading. This material is available free of charge via the Internet at http://pubs.acs.org.

■ AUTHOR INFORMATION

Corresponding Author

*E-mail: (L.S.S.) schadl@rpi.edu.

Notes

The authors declare no competing financial interest.

■ ACKNOWLEDGMENTS

The authors thank Prof. Sanat K Kumar, Ying Li, and Dr. Douglas Dukes for useful discussions. T.N. and B.C.B. would like to gratefully acknowledge the NSF (BME-1032579) for partial support of this work. B.N. and L.S.S. would like to gratefully acknowledge the Office of Naval Research (Grant No. N000141-01-02-4-4) for partial support of this work.

■ REFERENCES

(1) Witten, T. A.; Pincus, P. A. *Macromolecules* **1986**, *19*, 2509−2513.
(2) Taunton, H.; Toprakcioglu, C.; Fetters, L.; Klein, J. *Macromolecules* **1990**, *23*, 571−580.
(3) Balazs, A. C.; Emrick, T.; Russell, T. P. *Science (New York, N.Y.)* **2006**, *314*, 1107−10.
(4) Green, P. F. *Soft Matter* **2011**, *7*, 7914.
(5) Chevigny, C.; Jestin, J.; Gigmes, D.; Schweins, R.; Di-Cola, E.; Dalmas, F.; Bertin, D.; Boué, F. *Macromolecules* **2010**, *43*, 4833−4837.
(6) Green, P. F.; Oh, H.; Akcora, P.; Kumar, S. K. *Dynamics of Soft Matter*; García Sakai, V., Alba-Simionesco, C., Chen, S.-H., Eds.; Springer US: Boston, MA, 2012; pp 349−366.
(7) Maas, J. H.; Fleer, G. J.; Leermakers, F. A. M.; Cohen Stuart, M. A. *Langmuir* **2002**, *18*, 8871−8880.
(8) Akcora, P.; Liu, H.; Kumar, S. K.; Moll, J.; Li, Y.; Benicewicz, B. C.; Schadler, L. S.; Acehan, D.; Panagiotopoulos, A. Z.; Pryamitsyn, V.; Ganesan, V.; Ilavsky, J.; Thiyagarajan, P.; Colby, R. H.; Douglas, J. F. *Nat. Mater.* **2009**, *8*, 354−9.
(9) Pryamitsyn, V.; Ganesan, V.; Panagiotopoulos, A. Z.; Liu, H.; Kumar, S. K. *J. Chem. Phys.* **2009**, *131*, 221102.
(10) Ferreira, P. G.; Ajdari, A.; Leibler, L. *Macromolecules* **1998**, *31*, 3994−4003.
(11) Borukhov, I. *Macromolecules* **2002**, *35*, 5171−5182.
(12) Hasegawa, R.; Aoki, Y.; Doi, M. *Macromolecules* **1996**, *29*, 6656−6662.
(13) Kalb, J.; Dukes, D.; Kumar, S. K.; Hoy, R. S.; Grest, G. S. *Soft Matter* **2011**, *7*, 1418.
(14) Kumar, S. K.; Krishnamoorti, R. *Annu. Rev. Chem. Biomol. Eng.* **2010**, *1*, 37−58.
(15) Chevigny, C.; Dalmas, F.; Di Cola, E.; Gigmes, D.; Bertin, D.; Boué, F.; Jestin, J. *Macromolecules* **2011**, *44*, 122−133.
(16) Sunday, D.; Ilavsky, J.; Green, D. L. *Macromolecules* **2012**, *45*, 4007−4011.
(17) Akcora, P.; Kumar, S. K.; García Sakai, V.; Li, Y.; Benicewicz, B. C.; Schadler, L. S. *Macromolecules* **2010**, *43*, 8275−8281.
(18) Moll, J. F.; Akcora, P.; Rungta, A.; Gong, S.; Colby, R. H.; Benicewicz, B. C.; Kumar, S. K. *Macromolecules* **2011**, *44*, 7473−7477.
(19) Maillard, D.; Kumar, S. K.; Fragneaud, B.; Kysar, J. W.; Rungta, A.; Benicewicz, B. C.; Deng, H.; Brinson, L. C.; Douglas, J. F. *Nano Lett.* **2012**, *12*, 3909−14.
(20) Rungta, A.; Natarajan, B.; Neely, T.; Dukes, D.; Schadler, L. S.; Benicewicz, B. C. *Macromolecules* **2012**, *45*, 9303−9311.
(21) Li, Y.; Tao, P.; Viswanath, A.; Benicewicz, B. C.; Schadler, L. S. *Langmuir* **2013**, *29*, 1211−1220.
(22) Jayaraman, A. *J. Polym. Sci., Part B: Polym. Phys.* **2013**, *51*, 524−534.
(23) Kim, D.; Lee, J. S.; Barry, C. M. F.; Mead, J. L. *Microsc. Res. Tech.* **2007**, *70*, 539−546.
(24) Calebrese, C.; Hui, L.; Schadler, L.; Nelson, J. *IEEE Trans. Dielectr. Electr. Insul.* **2011**, *18*, 938−945.
(25) Williams, M. L.; Landel, R. F.; Ferry, J. D. *J. Am. Chem. Soc.* **1955**, *77*, 3701−3707.
(26) Pharr, G. M.; Oliver, W. C.; Brotzen, F. R. *J. Mater. Res.* **2011**, *7*, 613−617.
(27) Oliver, W. C.; Pharr, G. M. *J. Mater. Res.* **2004**, *19*, 3−20.
(28) Rinde, J. A. *J. Appl. Polym. Sci.* **1970**, *14*, 1913−1926.
(29) Trombly, D. M.; Ganesan, V. *J. Chem. Phys.* **2010**, *133*, 154904.
(30) Edgecombe, S. R.; Gardiner, J. M.; Matsen, M. W. *Macromolecules* **2002**, *35*, 6475−6477.
(31) Dodd, P. M.; Jayaraman, A. *J. Polym. Sci., Part B: Polym. Phys.* **2012**, *50*, 694−705.
(32) Vold, M. J. *J. Colloid Sci.* **1961**, *16*, 1−12.
(33) Cho, S.; Lee, S.; Hyun, J.; Paik, K. *J. Mater. Sci.* **2005**, *6*, 77−84.
(34) LaRue, I.; Adam, M.; Pitsikalis, M.; Hadjichristidis, N.; Rubinstein, M.; Sheiko, S. S. *Macromolecules* **2006**, *39*, 309−314.
(35) Minko, S. *J. Macromol. Sci.* **2006**, *46*, 397−420.
(36) Aubouy, M.; Fredrickson, G.; Pincus, P.; Raphaeel, E. *Macromolecules* **1995**, *28*, 2979−2981.
(37) Raphael, E.; Pincus, P.; Fredrickson, G. *Macromolecules* **1993**, 1996−2006.
(38) Milner, S.; Witten, T.; Cates, M. *Macromolecules* **1988**, *21*, 2610−2619.
(39) Mewis, J.; Frith, W. J.; Strivens, T. A.; Russel, W. B. *AIChE J.* **1989**, *35*, 415−422.
(40) Zhulina, E. B.; Adam, M.; LaRue, I.; Sheiko, S. S.; Rubinstein, M. *Macromolecules* **2005**, *38*, 5330−5351.
(41) Halpin, J. C.; Kardos, J. L. *Polym. Eng. Sci.* **1976**, *16*, 344−352.
(42) Guth, E. *J. Appl. Phys.* **1945**, *16*, 20.
(43) Wu, Y.-P.; Jia, Q.-X.; Yu, D.-S.; Zhang, L.-Q. *Polym. Test.* **2004**, *23*, 903−909.
(44) Schadler, L. S.; Kumar, S. K.; Benicewicz, B. C.; Lewis, S. L.; Harton, S. E. *MRS Bull.* **2007**, *32*, 335−340.
(45) Montes, H.; Chaussée, T.; Papon, a; Lequeux, F.; Guy, L. *Eur. Phys. J. E, Soft Matter* **2010**, *31*, 263−8.
(46) Lee, H.; Ahn, H.; Naidu, S.; Seong, B. S.; Ryu, D. Y.; Trombly, D. M.; Ganesan, V. *Macromolecules* **2010**, *43*, 9892−9898.
(47) Bansal, A.; Yang, H.; Li, C.; Benicewicz, B. C.; Kumar, S. K.; Schadler, L. S. *J. Polym. Sci., Part B: Polym. Phys.* **2006**, *44*, 2944−2950.
(48) Schneider, H. A.; Di Marzio, E. A. *Polymer* **1992**, *33*, 3453−3461.
(49) Oh, H.; Green, P. F. *Nature Mater.* **2009**, *8*, 139−43.
(50) Smith, G. D.; Bedrov, D.; Li, L.; Byutner, O. *J. Chem. Phys.* **2002**, *117*, 9478.
(51) Dukes, D.; Li, Y.; Lewis, S.; Benicewicz, B.; Schadler, L.; Kumar, S. K. *Macromolecules* **2010**, *43*, 1564−1570.